AIP | Review of Scientific Instruments

# Q-band 4-state phase shifter in planar technology: Circuit design and performance analysis

E. Villa, J. Cagigas, B. Aja, L. de la Fuente, and E. Artal

Citation: Review of Scientific Instruments **87**, 094705 (2016); doi: 10.1063/1.4963322
View online: http://dx.doi.org/10.1063/1.4963322
View Table of Contents: http://scitation.aip.org/content/aip/journal/rsi/87/9?ver=pdfcov
Published by the AIP Publishing

**Articles you may be interested in**

Low noise, 0.4–3 GHz cryogenic receiver for radio astronomy
Rev. Sci. Instrum. **85**, 104710 (2014); 10.1063/1.4900446

Design methodology and performance analysis of a wideband 90° phase switch for radiometer applications
Rev. Sci. Instrum. **84**, 124704 (2013); 10.1063/1.4849555

Nanoscale spin wave valve and phase shifter
Appl. Phys. Lett. **100**, 172408 (2012); 10.1063/1.4705289

Flexoelectric phase shifter for spin waves
J. Appl. Phys. **111**, 083907 (2012); 10.1063/1.4703925

UNIVERSAL SCALING LAW OF INERTANCE TUBE PHASE SHIFTER
AIP Conf. Proc. **985**, 1075 (2008); 10.1063/1.2908456


Reuse of AIP Publishing content is subject to the terms at: https://publishing.aip.org/authors/rights-and-permissions. Download to IP: 193.144.201.248 On: Thu, 29 Sep 2016 13:36:19

# Q-band 4-state phase shifter in planar technology: Circuit design and performance analysis

E. Villa,[1,a)] J. Cagigas,[2] B. Aja,[1] L. de la Fuente,[1] and E. Artal[1]
[1]*Department of Communications Engineering, University of Cantabria, Plaza de la Ciencia s/n, Santander 39005, Spain*
[2]*Erzia Technologies, Josefina de la Maza 4, Santander 39012, Spain*

(Received 22 June 2016; accepted 12 September 2016; published online 29 September 2016)

A 30% bandwidth phase shifter with four phase states is designed to be integrated in a radio astronomy receiver. The circuit has two 90° out-of-phase microwave phase-shifting branches which are combined by Wilkinson power dividers. Each branch is composed of a 180° phase shifter and a band-pass filter. The 180° phase shifter is made of cascaded hybrid rings with microwave PIN diodes as switching devices. The 90° phase shift is achieved with the two band-pass filters. Experimental characterization has shown significant results, with average phase shift values of −90.7°, −181.7°, and 88.5° within the operation band, 35–47 GHz, and mean insertion loss of 7.4 dB. The performance of its integration in a polarimetric receiver for radio astronomy is analyzed, which validates the use of the presented phase shifter in such type of receiver. *Published by AIP Publishing.* [http://dx.doi.org/10.1063/1.4963322]

## I. INTRODUCTION

The design of phase switching circuits has been a significant task over decades since they define the performance of multiple communication systems. Additionally, their performances are needed to be particularly outstanding when wideband applications are considered. The latter scenario is applied in radio astronomy, in which great bandwidths together with low-noise circuits are employed in order to obtain the most sensitive receivers.[1] But also the performance of the phase switching devices defines the receiver quality, since high errors in phase or amplitude responses between states imply a reduction in the scientific goals.[2] Common required features for the phase switching circuits are flat phase response over the bandwidth and low in-band amplitude imbalance and phase error between states.

The proposed circuit is part of a radio astronomy receiver intended for characterizing the Cosmic Microwave Background (CMB) polarization in the 35–47 GHz frequency band.[1] Some phase shifter solutions working at Q-band have been implemented using several technologies,[3–15] such as monolithic microwave integrated circuit (MMIC) or microelectromechanical systems (MEMS), in which transmission line topologies with active devices are used to achieve the phase shift at a single frequency or over a couple of gigahertz bandwidths with the exception of one broadband design in Ref. 4. All these designs show good phase performances with low phase errors and root-mean-square (RMS) phase errors better than 11.3°.

This work describes the design and characterization of a wideband four phase states hybrid planar technology phase shifter based on PIN diodes. The proposed solution shows a competitive performance facing Q-band MMIC designs, with a relative bandwidth of 30% and significantly low RMS phase and amplitude errors within the band. Besides, it overcomes the high production costs and long manufacturing times of MMIC solutions.

Moreover, the performance analysis of a pixel for the Forty Gigahertz Instrument (FGI) receiver[16,17] is described, and the efficiency of the phase switch circuit in the system, which is part of its back-end module, is validated. For such analysis, a simplified version of the back-end is assumed, and the impact of the phase switch is calculated in terms of the phase errors in the output signals when the circuit state is modified.

The document is divided into five sections. An introduction is presented in the first section while the second one defines the design of the phase switch circuit, describing the different circuit parts and the full circuit performance. The experimental results are presented and discussed in Section III. The impact of the designed circuit as part of a radio astronomy receiver is analyzed in Sec. IV, and finally, Section V draws general conclusions.

## II. CIRCUIT ANALYSIS AND DESIGN

The phase switching circuit design is intended for ensuring two main issues in order to provide overall significant performance of a hybrid solution. First of all, it must consider a high integration level with other subsystems. Besides, it must ensure minimum interconnections between the elements which compose the circuit, since they are critical for the whole module performance at these frequencies. Therefore, the design is fully developed in microstrip technology, allowing a complete integration of the subsystems which compose the full shifting structure. And, moreover, this solution only requires external interconnection elements at its input and output accesses.

The schematic of the phase switch design is shown in Fig. 1. The circuit is composed of three parts: a Wilkinson

a)Author to whom correspondence should be addressed. Electronic mail: villae@unican.es.


Reuse of AIP Publishing content is subject to the terms at: https://publishing.aip.org/authors/rights-and-permissions. Download to IP: 193.144.201.248 On: Thu, 29 Sep 2016 13:36:19

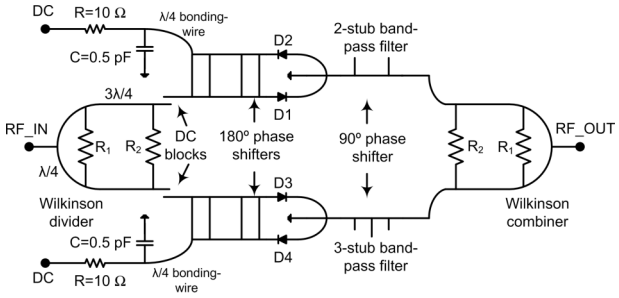


FIG. 1. Schematic of the 4-state phase switching circuit.

power splitter, a 180° phase shifter, and a 90° phase shifter. All the planar structures are implemented in microstrip technology on alumina substrate, and the switching devices for the 180° phase shifter are microwave PIN diodes.

### A. Principle of operation

The circuit is composed of two phase shifting branches, whose insertion phases differ 90°. Besides, both branches are able to modify 180° its individual insertion phase by activating the switching devices in the circuit. The branches are joined by power splitters at both accesses, which split and combine the individual signals travelling by each branch. Then the proper combination of the branches state produces the 90°, 180° or 270° differential phase states in the circuit related to the reference phase state.

The phase state of the circuit is described in Table I, in which the set of diodes used in the circuit (D1, D2, D3, and D4 in Fig. 1) is switched between the ON and OFF states of each diode. The ON state of each diode is considered when a positive bias voltage is applied to their anodes, so the PIN diodes are behaving as a low series resistance. When a negative voltage is applied, the OFF state is considered, and the equivalent circuit of the diode is a series capacitance.

### B. Wilkinson power splitter

The signal is divided and combined with microstrip Wilkinson structures. In order to cover properly the bandwidth, a two section design is implemented, using the resistive layer of the alumina substrate for directly etching the resistors over the substrate.[18] The stepped effect in the series transmission lines adds an extra electrical length which should be corrected in the transmission line length. The shortening for the second quarter-wavelength line makes the cascaded assembly of the circuits unfeasible, therefore this second stage is performed using a three quarter-wavelength line instead of the quarter-wavelength one.

TABLE I. Relative phase state of the circuit depending on the bias point of each diode.

| Relative phase state | D1 state | D2 state | D3 state | D4 state |
|---|---|---|---|---|
| Reference – 0° | ON | OFF | ON | OFF |
| 90° | OFF | ON | ON | OFF |
| 180° | ON | OFF | OFF | ON |
| 270° | OFF | ON | OFF | ON |

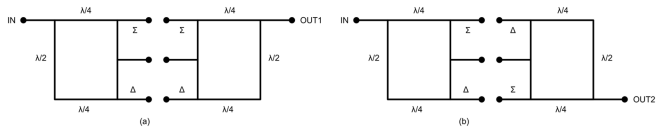


FIG. 2. Diagram to show the feasible connections of the back-to-back hybrid rings. (a) Directly connecting adding outputs. (b) Connecting sum to difference outputs.

### C. 180° phase switch circuit

The design is based on the proposal described in Ref. 19, which combines two cascaded rat-race couplers to achieve a flat phase response between states over the bandwidth. This proposal cascades two 180° hybrid splitters by connecting 3 of their arms between them, as shown in Fig. 2: the second access and the sum and difference outputs are directly connected to the corresponding accesses of the second hybrid. Consequently, the back-to-back connection of the hybrids shows two feasible alternatives: directly connecting their adding and difference outputs between them (Fig. 2(a)) or joining the sum outputs to the difference ones (Fig. 2(b)). These two connections individually analyzed provide a phase difference between them of 180° within the operating bandwidth. Therefore, the combination of these two performances on a single circuit in order to achieve a 180° phase shift is designed and implemented, using switching devices placed at each output access, labelled OUT1 and OUT2 in Fig. 2, in order to select the corresponding output.

The proposed circuit uses modified cascaded hybrid rings, adding an extra section to provide wider bandwidth. A schematic circuit to explain its operation is shown in Fig. 3, considering only one of the 180° phase shifters in Fig. 1. By mean of a series pair of diodes in opposite configuration assembly, the microwave signal is guided by the upper or lower transmission path depending on the bias point of the D1-D2 diodes. Therefore, the difference on the phase is 180° over the desired bandwidth when comparing both signals. Additionally, a single DC bias signal is needed to bias the set of diodes.

The designed circuit, after an optimization process, is shown in Fig. 4(a). The performance in terms of the S-parameters and the phase difference between states is also depicted in Fig. 4.

### D. 90° fixed phase shifter

The 90° phase shifter is configured with two microstrip band-pass filters. Their goal is that their insertion phase differs 90° over the bandwidth as well as with minimum amplitude

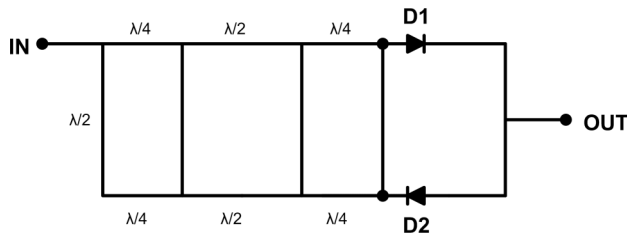


FIG. 3. Circuit schematic of the 180° phase switch circuit with the diodes and the electrical lengths.

Reuse of AIP Publishing content is subject to the terms at: https://publishing.aip.org/authors/rights-and-permissions. Download to IP: 193.144.201.248 On: Thu, 29 Sep 2016 13:36:19

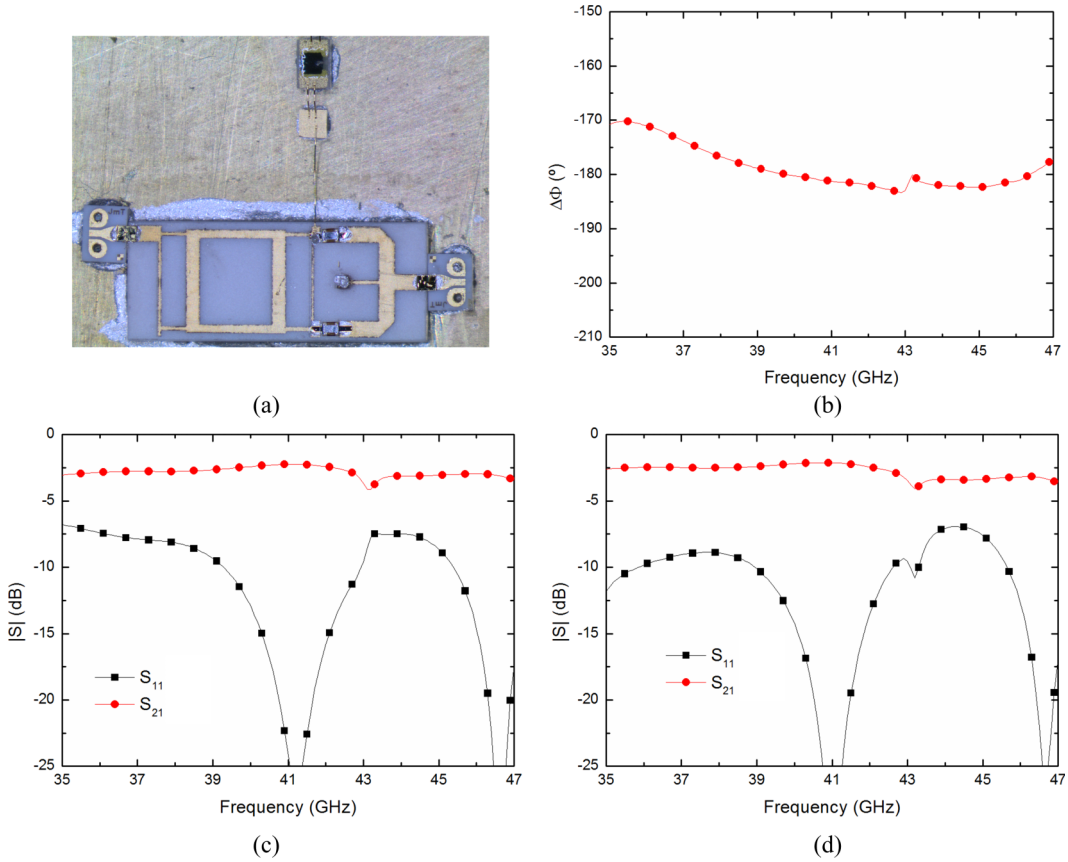


FIG. 4. 180° phase switch circuit measured performance. (a) Photograph of the circuit on alumina. (b) Phase difference between both states. (c) S-parameters in its first state. (d) S-parameters in its second state.

imbalance between them. Both filters are based on the use of cascaded π-networks.[20] Each filter is placed in a different circuit branch of the 4-state phase switching circuit, as it is shown in Fig. 1, providing a fixed 90° phase difference between branches.

The filters are individually manufactured and characterized in a coplanar probe station, and their results, in terms of the S-parameters of each one and the phase difference between them, are shown in Fig. 5, as well as a photograph of each filter.

### E. Circuit simulation performance

The whole circuit performance is evaluated using an electromagnetic simulator for all the passive structures and an

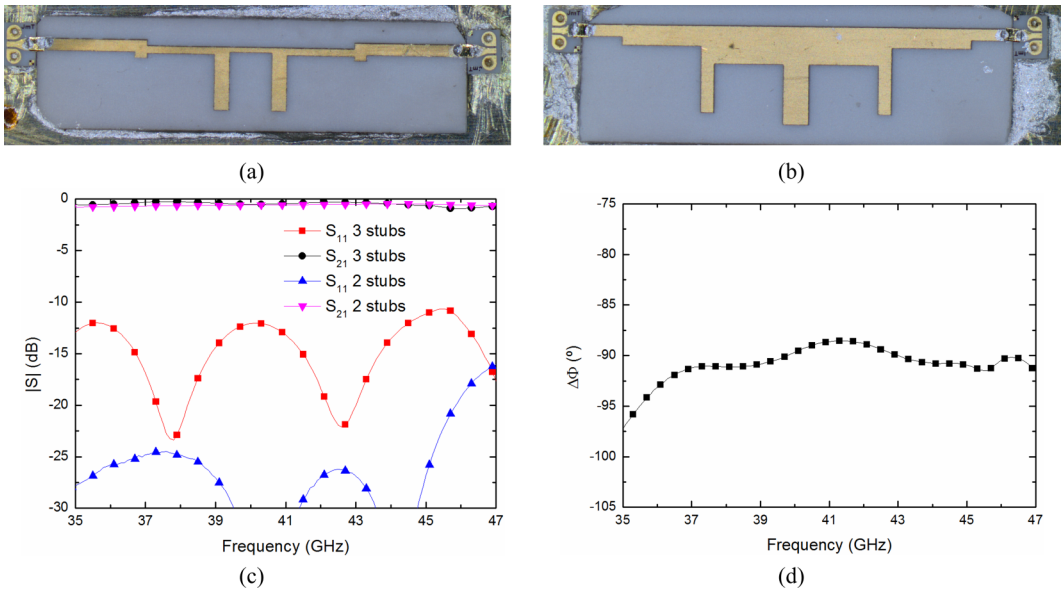


FIG. 5. 90° phase shifter performance. (a) Photograph of the 2 open-ended stub filter on alumina. (b) Photograph of the 3 open-ended stub filter. (c) S-parameters of each filter. (d) Phase difference of each filter.

Reuse of AIP Publishing content is subject to the terms at: https://publishing.aip.org/authors/rights-and-permissions. Download to IP: 193.144.201.248 On: Thu, 29 Sep 2016 13:36:19

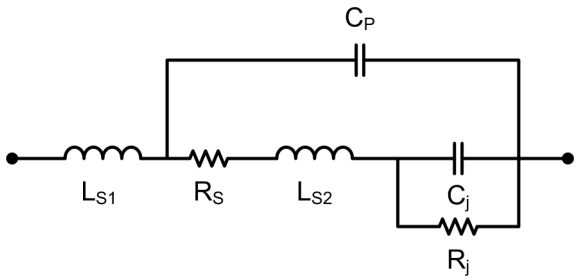


FIG. 6. Small signal model for the HPND-4005 diode.

extrapolated small-signal model for the diode up to 50 GHz.[20] The switching devices for the 180° phase shifter are microwave PIN diodes, the HPND-4005 device from Avago Technologies. The small signal model employed in the design is shown in Fig. 6, and its element values are listed in Table II. As described in Ref. 12, the resistors $R_S$ and $R_j$ are defined by

$$R_S = R_{SI\text{-}V} + \frac{A}{(I_{bias} + 1{\cdot}10^{-14})^K}, \quad (1)$$

$$R_j = \frac{n \cdot k \cdot T}{q} \cdot \frac{1}{(I_{bias} + I_S)}, \quad (2)$$

which values depend on the bias points of the diode, and $n$ is the ideality factor, $I_S$ the saturation current, $k$ the Boltzmann constant, $T$ the physical absolute temperature (297 K), $q$ the electron charge ($1.6 \times 10^{-19}$ C), $I_{bias}$ the bias point, and $A$ and $K$ two constants. The values of these parameters are listed in Table III.

A sample of diodes has been measured in order to extract the model, showing a small spread between their results, and in a very good fitting with the extracted model.

The substrate used for the design is 10-mil thick alumina: dielectric constant $\varepsilon_r = 9.9$, metallization thickness 3 $\mu$m, and a 50 Ω/square tantalum-nitride resistive layer. Besides, the DC circuitry is also included to avoid any circuit mismatching due to the DC network. The phase simulation results are shown in Fig. 7, in which the phase shifts for each state are depicted related to the reference one. The simulations show an average phase shifts over the 35–47 GHz bandwidth of −91.7°, 92.1°, and 179.1°.

## III. EXPERIMENTAL CHARACTERIZATION

A complete phase switching circuit is manufactured and assembled in order to be characterized in amplitude and phase. A picture of the manufactured circuit is shown in Fig. 8. Microstrip-to-coplanar commercial transitions are used at circuit accesses, whose effect is removed after a standard calibration technique.

TABLE II. Parameters of the small signal model for the HPND-4005 diode.

| Parameter | Value |
|---|---|
| $L_{S1}$ | 130 pH |
| $L_{S2}$ | 165 pH |
| $C_P$ | 0.035 pF |
| $C_j$ | 0.024 pF |

TABLE III. Parameters of the I-V curve of the HPND-4005 diode.

| Parameter | Value |
|---|---|
| $n$ | 2.08 |
| $I_S$ | $4.37 \times 10^{-10}$ A |
| $R_{SI\text{-}V}$ | 0.85 Ω |
| $A$ | 0.25 |
| $K$ | 0.307 |

A microstrip single section coupled lines DC block[21] is added to the circuit at the input of each 180° phase shifter to be properly biased. A detailed view of the DC block is also shown in Fig. 8. The total power consumption of the circuit is 48 mW, with 20 mA per forward biased diode.

The measurements of the circuit are performed in the frequency band from 35 to 47 GHz. It is measured in a coplanar probe station using a PNA E8364A from Keysight Technologies. Two DC bias signals are used to change individually the state of each branch. The two 180° phase switches include their bias network, which is composed of a quarter-wavelength bond wire at the center frequency (41 GHz), a 0.5 pF single layer capacitor to ground, and a 10 Ω series resistor. The scattering parameters are measured for each state, and their performances are shown in Fig. 9 in solid lines with filled symbols, compared to the simulations of the circuit (outlined symbols). They show an average insertion loss of 7.4 dB, whereas return loss better than 7 dB at the input and 9 dB at the output in the 35–47 GHz band. Meanwhile, return loss better than 7 dB at the input and 11 dB at the output with mean insertion loss of 7 dB in the frequency band. The phase shifts for each state are calculated comparing the measurement of the insertion phase of each state to the reference one, and the results are shown in Fig. 10. Mean phase shifts of −90.7°, 88.5°, and −181.7° are measured in the band of interest.

The root-mean-square (RMS) phase and amplitude deviations are calculated, and they are shown in Fig. 11. The RMS phase error is measured to be less than 8°, whereas the RMS amplitude error is lower than 1.6 dB in the frequency band. The overall response is affected by the combination of all the subsystems, and higher RMS error is achieved when poor return loss is measured in the circuit.

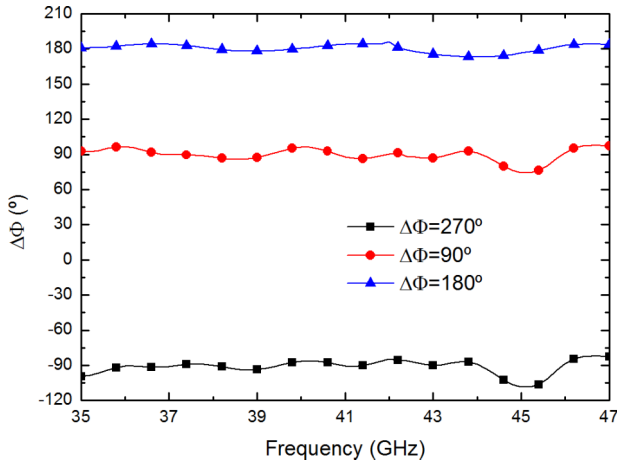


FIG. 7. Simulated phase shifts for the 3 different phase states related to the reference state.

Reuse of AIP Publishing content is subject to the terms at: https://publishing.aip.org/authors/rights-and-permissions. Download to IP: 193.144.201.248 On: Thu, 29 Sep 2016 13:36:19

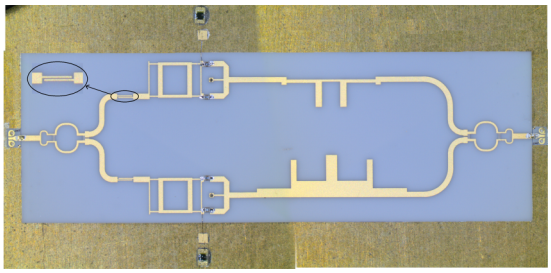

FIG. 8. Photograph of the phase switching circuit. Dimensions: 24.8 × 8.1 × 0.254 mm$^3$.

Finally, Table IV shows performance comparisons of the phase switching circuit described in this work with other reported technologies Q- and other frequency bands phase switching structures. The design presented in this work shows wider operating bandwidth than most of the referenced works; the circuit provides very flat phase shifts over the 30% required bandwidth. Besides, this work provides RMS phase and amplitude errors better than or comparable to other MMIC solutions.

## IV. POLARIMETRIC RECEIVER: INTEGRATION, ANALYSIS, AND DISCUSSION

The phase switching circuit is part of the FGI Q-U-I Joint Tenerife Experiment (QUIJOTE) receiver, whose receiver scheme is shown in Fig. 12. The instrument is intended for characterizing the Cosmic Microwave Background (CMB) polarization by measuring three of the Stokes parameters ($Q$, $U$, and $I$) simultaneously. The receiver is composed of two microwave circuit branches per feedhorn antenna, which are correlated and detected in the last module of the full chain. The phase modulation introduced by the phase switches module

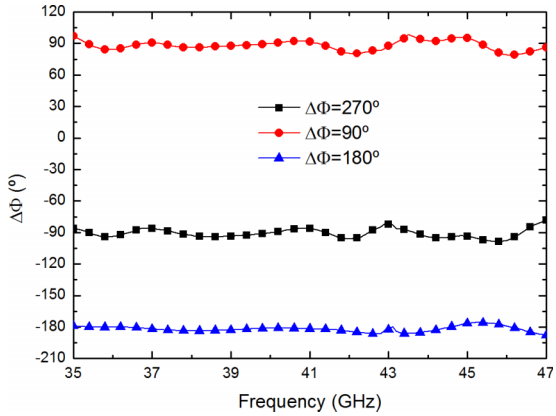


FIG. 10. Measured phase shifts for the 3 different phase states related to the reference state.

enables the reduction of the systematic errors in the receiver, the overcoming of the 1/f noise with a proper modulation frequency and the minimization of the leakage among the Stokes parameters calculation.

Therefore, the amplitude and phase errors introduced by the phase switch circuit are needed to be analyzed in order to estimate their influence in the receiver functionality. Hence, an analysis of the receiver behavior considering the measured results of the phase switching circuit is performed. A simplified version of the scheme shown in Fig. 12 is taken into account for the analysis, in which only the phase switches and the correlation and detection modules are used, as shown in the scheme of Fig. 13. This reduced receiver configuration is fully representative of the pixel functionality, since the low noise amplifiers (LNA) are chosen to be paired with similar insertion phases, minimizing the phase deviation between them. Besides,

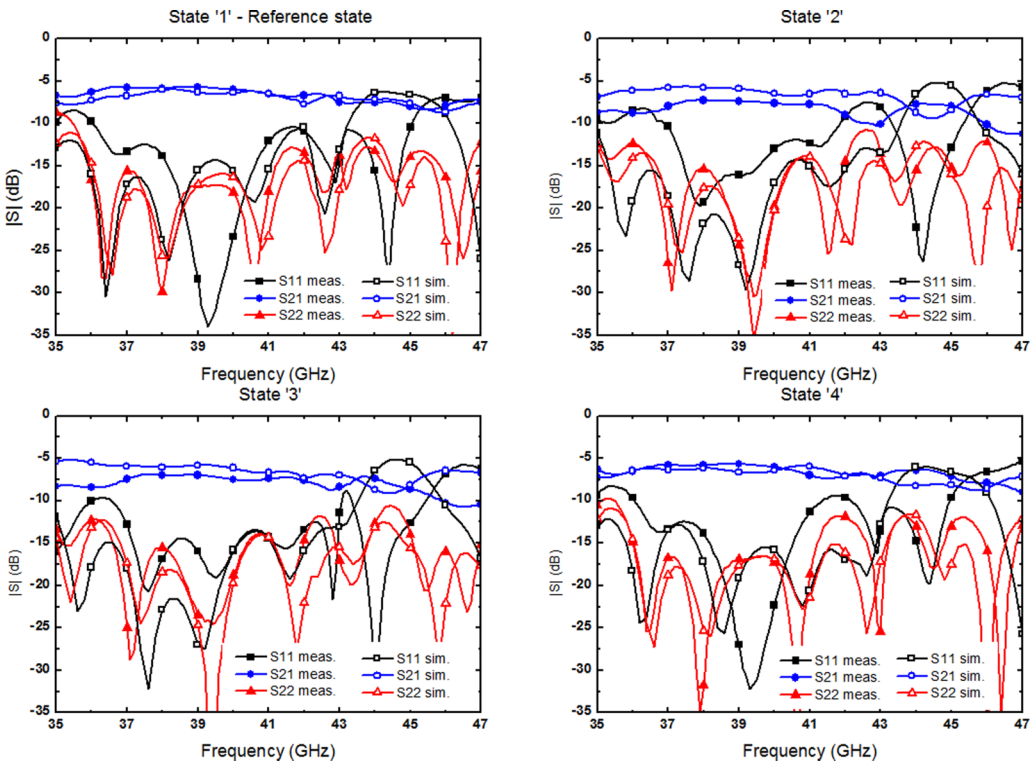


FIG. 9. Simulated and measured S-parameters of the circuit for the 4 states.

Reuse of AIP Publishing content is subject to the terms at: https://publishing.aip.org/authors/rights-and-permissions. Download to IP: 193.144.201.248 On: Thu, 29 Sep 2016 13:36:19

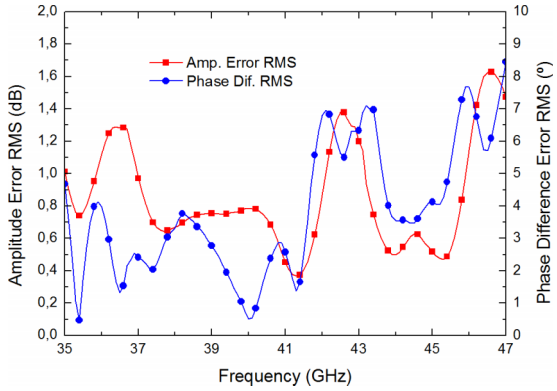


FIG. 11. Measured RMS amplitude and phase errors versus frequency.

the minimum conceivable phase difference provided by the amplification stages will be corrected using adjusting phase components. The phase switches module shown in the figure is composed of two phase switching circuits identical to the one described above, each one assembled in a branch of the module.

The analysis is based on the use of a correlation and detection module model performing variations in the phase state of the phase switches module. The model of the correlation and detection module is based on the electromagnetic performances of WR22 waveguide structures (90° broadband hybrids and 90° phase shifter), Schottky diode detectors to achieve the signal conversion and DC amplification. When the phase switches module is operating on its reference state, the correlation and detection module is expected to be excited with two in-phase equal amplitude signals and provides at their outputs DC signals of maximum level ($V_{max}$) in $V_{d1}$, two mid-level ($V_{med1}$, $V_{med2}$) in $V_{d3}$ and $V_{d4}$, and a minimum level ($V_{min}$) in $V_{d2}$. In the particular case of no amplitude or phase errors between the incoming signals to the detectors, the two mid-level signals show the same amplitude level ($V_{d3} = V_{d4}$). Besides, the sum of the maximum and minimum DC signals is equal to the sum of the two mid-level DC signals ($V_{d1} + V_{d2} = V_{d3} + V_{d4}$). When the phase switches module changes its phase state, the position of the maximum, minimum, and mid-level voltages varies in the labelled output signals ($V_{d1}$–$V_{d4}$).

To evaluate the effect of the different phase states on the receiver performance, two parameters are defined: the root mean square error, *RMS_M*, of the differences between the $V_{max}$ and $V_{min}$ related to each mid-level voltages, and the isolation between mid-level voltages, *ISO_M*. The *RMS_M* is defined as

$$RMS\_M = \sqrt{\frac{VD\_1^2 + VD\_2^2}{2}}, \tag{3}$$

where RMS_1 and RMS_2 are the relative error regarding each mid-level DC output per state, which are given by

$$VD\_1 = \frac{V_{max} - V_{med1}}{V_{med1} - V_{min}} - 1, \tag{4}$$

$$VD\_2 = \frac{V_{max} - V_{med2}}{V_{med2} - V_{min}} - 1. \tag{5}$$

On the other hand, *ISO_M* is defined as the modulus of the magnitude, in dB, of the difference between the two mid-level voltages, expressed as

$$ISO\_M = \left|10 \cdot \log_{10}\left(|V_{med1} - V_{med2}|\right)\right|. \tag{6}$$

This second parameter stresses the effect of the error, since, ideally, the two mid-level voltages should be equal, and when relevant deviations between them are involved, a low figure is expected for *ISO_M*.

In an ideal receiver the ratio *RMS_M* and *ISO_M* should be equal to 0 and infinity, respectively. Isolation values greater than 10 dB and minimum achievable root mean square error are desired in the receiver analysis in order to consider a proper performance. In case of not accomplishment of required isolation, the calculation of the Stokes parameters will be inaccurate.

According to the scheme in Fig. 13, the combination of the phase states in each phase switches module branch provides 16 phase states in the receiver. Since they are combinations of the same phase states in each branch, the pixel shows four redundant states (0°, 90°, 180°, and 270°). Therefore, the analysis of the phase state of the pixel can be reduced to the analysis of the equivalent phase state, defined as the difference among the individual phase states of each branch.

TABLE IV. Comparison of wideband multi-state phase shifters.

| Reference | Frequency (GHz) | Phase states | RMS phase error (°) | Phase error (°) | RMS amplitude error (dB) | Technology |
|---|---|---|---|---|---|---|
| 3 | 46-49 | 16 | <7.6 | … | <1.2 | MMIC InGaAs |
| 4 | 32-50 | 16 | <8.7 | … | <1.2 | MMIC SiGe |
| 5 | 40-45 | 16 | <8.8 | … | <1.3 | MMIC SiGe |
| 6 | 39-42 | 16 | <11.3 | … | <5 | MMIC CMOS |
| 7 | 44-46 | 16 | … | … | <0.7 | MMIC SiGe |
| 8 | 10.25 | 4 | … | ±2 | … | MEMS |
| 9 | 37.7 | 4 | … | <1 | … | DMTL MEMS |
| 10 | 81 | 4 | … | 2 | … | MEMS |
| 11 | 60 | 4 | … | <1 | … | Switched line MEMS |
| 12 | 20 | 4 | … | <14 | … | DMTL MEMS |
| 13 | 60 | 4 | … | 5.7 | … | Reflection-type MEMS |
| 14 | 90 | 4 | … | <10 | … | MMIC CMOS |
| 15 | 60 | 4 | … | <15 | … | MEMS |
| This work | 35-47 | 4 | <8 | <2 | <1.6 | Hybrid PIN diodes |

Reuse of AIP Publishing content is subject to the terms at: https://publishing.aip.org/authors/rights-and-permissions. Download to IP: 193.144.201.248 On: Thu, 29 Sep 2016 13:36:19

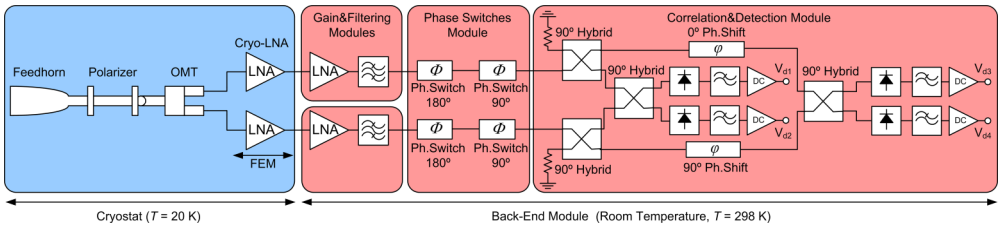


FIG. 12. Sketch of the FGI QUIJOTE receiver.

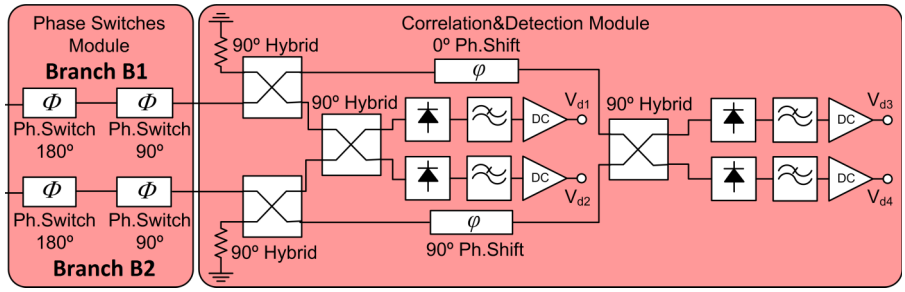


FIG. 13. Simplified sketch of the FGI QUIJOTE receiver for the impact analysis of the phase switch circuit imbalances.

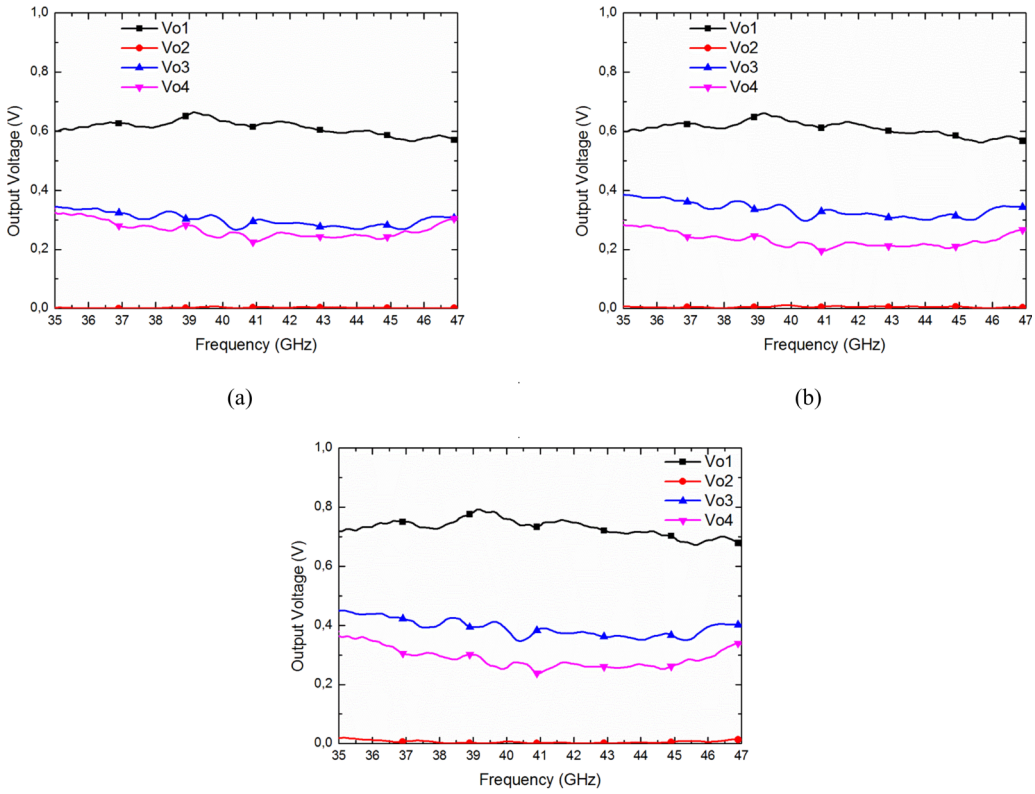


FIG. 14. Impact of the phase and amplitude imbalances using the correlation and detection module model. (a) No phase nor amplitude imbalances at the correlation module inputs. (b) 7° phase error between correlation module inputs. (c) 5° phase error and 1.5 dB amplitude imbalance between correlation module inputs.

Hence, the initial approach is to consider the correlation and detection module defined by real simulations. The model of that module takes into account both 90° waveguide hybrids isolation and mismatching effects between circuits, as well as the phase and amplitude errors of the 90° fixed waveguide phase shifter. Therefore, its isolation is restricted, and its flaws are considered as initial values for *RMS_M* and *ISO_M*.

A first analysis of the phase states presented at the inputs of the correlation and detection module involves applying flat phase (0°, 90°, 180°, and 270°) and amplitude (equivalent insertion loss of the measured circuit) over the frequency band at those inputs. Then a second analysis is performed with the different phase states at the input of the correlator, considering the measured phase states provided by the phase switch circuit

Reuse of AIP Publishing content is subject to the terms at: https://publishing.aip.org/authors/rights-and-permissions. Download to IP: 193.144.201.248 On: Thu, 29 Sep 2016 13:36:19

TABLE V. Values for the *RMS_M* and *ISO_M* from the output signals by applying measured phase states.

| Phase state B1 | Phase state B2 | Relative phase state | $RMS\_M_{sim}$ | $ISO\_M_{sim}$ (dB) | $RMS\_M_{measurements}$ | $ISO\_M_{measurements}$ (dB) |
|---|---|---|---|---|---|---|
| 0° | 0° | 0° | 0.222 | 14.614 | 0.240 | 15.406 |
| | 90° | 90° | 0.171 | 20.835 | 0.181 | 19.136 |
| | 180° | 180° | 0.228 | 14.226 | 0.236 | 15.256 |
| | 270° | 270° | 0.167 | 23.024 | 0.175 | 39.333 |
| 90° | 0° | 270° | 0.167 | 23.028 | 0.177 | 21.244 |
| | 90° | 0° | 0.222 | 14.619 | 0.220 | 13.818 |
| | 180° | 90° | 0.171 | 20.835 | 0.181 | 23.385 |
| | 270° | 180° | 0.228 | 14.228 | 0.187 | 16.066 |
| 180° | 0° | 180° | 0.228 | 14.226 | 0.260 | 14.364 |
| | 90° | 270° | 0.167 | 23.024 | 0.184 | 16.309 |
| | 180° | 0° | 0.222 | 14.614 | 0.240 | 15.060 |
| | 270° | 90° | 0.171 | 20.835 | 0.181 | 26.369 |
| 270° | 0° | 90° | 0.171 | 20.835 | 0.195 | 16.621 |
| | 90° | 180° | 0.228 | 14.228 | 0.290 | 11.688 |
| | 180° | 270° | 0.167 | 23.028 | 0.179 | 20.775 |
| | 270° | 0° | 0.222 | 14.619 | 0.226 | 13.784 |

presented above. All the approaches provide four DC output signals per phase state.

The first analysis considers flat phase or amplitude differences at the inputs of the correlation and detection module, and Fig. 14(a) depicts the imbalance of the two mid-level voltages versus frequency due only to the phase and amplitude imbalances of the correlation and detection module model. On the other hand, Figs. 14(b) and 14(c) show how the mid-voltages deteriorate with respect to the initial situation in a fixed state (*Phase State B*1 = *Phase State B*2 = 0°), when a single 7° phase error within the band and combined errors of 5° in phase and 1.5 dB in amplitude are introduced in one branch of the receiver regarding the other at the input of the correlation unit. The values of isolation, *ISO_M*, are 9.88 dB and 9.87 dB, respectively, for the analyzed situations, which are below the required value of 10 dB for suitable performance. The isolation affects the two mid-level voltages in the receiver, which are identical for the ideal case of perfect isolation.

Afterwards, the second analysis is performed using the measured performance of the phase switching circuit, providing the four DC output signals per phase state and their mean values over the bandwidth are calculated.

Consequently, the *RMS_M* and *ISO_M* values for the analysis of the receiver, in terms of the modification of the phase state of the system introducing a flat balanced phase shift, are calculated and listed in Table V in the columns $RMS\_M_{sim}$ and $ISO\_M_{sim}$. Then the parameter values, *RMS_M* and *ISO_M*, when applying the measured response of the described phase switching circuit, are obtained, which are listed in Table V, columns $RMS\_M_{measurements}$ and $ISO\_M_{measurements}$.

These results show a negligible variation in the detected voltages when real amplitude and phase imbalance of the phase switches module are applied to the receiver, providing for all the states isolations greater than 10 dB. This analysis supports that the circuit is suitable for the required receiver performance and validates it as an adequate part of the receiver. Therefore, the further calculation of the Stokes parameters, which the system is intended for, will be accurate.

## V. CONCLUSION

A Q-band four state phase switching circuit designed in hybrid technology using PIN diodes has been described. Three different wideband circuits have been designed as part of the switching circuit in microstrip technology, which enables full integration. The outstanding flat phase performance of the circuit has shown mean values of −90.7°, 88.5°, and −181.7° over the 35–47 GHz frequency band, with RMS phase and amplitude deviations lower than 8° and 1.6 dB, respectively. The circuit has shown return losses better than 7 dB at the input and 9 dB at the output within the band, with mean insertion loss of 7.4 dB. The simulated performance of the back-end module receiver with actual measurements of the presented phase switch validates the use of this phase switching circuit in a radio astronomy receiver covering the referred bandwidth. When the amplitude and phase imbalances of the circuit are included in the receiver, isolation and root mean square error values calculated from the output voltages in the different states guarantee suitable receiver performance.

## ACKNOWLEDGMENTS

This work was supported by the Ministerio de Economía y Competitividad, Spain, under the CONSOLIDER-INGENIO 2010 programme under the Reference No. CSD2010-00064. The authors would like to thank Eva Cuerno, with the Department of Communications Engineering, for her assistance in circuit assembly.

[1]E. Villa, J. L. Cano, J. Cagigas, D. Ortiz, F. J. Casas, A. R. Pérez, B. Aja, J. V. Terán, L. de la Fuente, E. Artal, R. Hoyland, and A. Mediavilla, Rev. Sci. Instrum. **86**, 024702 (2015).
[2]F. J. Casas, D. Ortiz, E. Villa, J. L. Cano, J. Cagigas, A. R. Pérez, B. Aja, J. V. Terán, L. de la Fuente, E. Artal, R. Hoyland, and R. Génova-Santos, Sensors **15**, 19124 (2015).

Reuse of AIP Publishing content is subject to the terms at: https://publishing.aip.org/authors/rights-and-permissions. Download to IP: 193.144.201.248 On: Thu, 29 Sep 2016 13:36:19

[3]M. Kim, J. G. Yang, and K. Yang, Electron. Lett. **46**, 225 (2010).
[4]K. W. Koh and G. M. Rebeiz, IEEE Trans. Microwave Theory Tech. **56**, 2046 (2008).
[5]K. W. Koh, J. W. May, and G. M. Rebeiz, IEEE J. Solid-State Circuits **44**, 1498 (2009).
[6]J. H. Kim and J. W. Lee, Microwave Opt. Technol. Lett. **55**, 2676 (2013).
[7]C. Y. Kim, D. W. Kang, and G. M. Rebeiz, IEEE Trans. Microwave Theory Tech. **60**, 730 (2012).
[8]G. L. Tan, R. E. Mihailovich, J. B. Hacker, J. F. DeNatale, and G. M. Rebeiz, IEEE Trans. Microwave Theory Tech. **51**, 297 (2003).
[9]J. S. Hayden and G. M. Rebeiz, in *IEEE MTT-S International Microwave Symposium Digest*, *Seattle, USA*, *2-7 June 2002* (IEEE, 2002), pp. 337–340.
[10]J. J. Hung, L. Dussopt, and G. M. Rebeiz, in *33rd European Microwave Conference*, *Munich, Germany*, *October 2003* (IEEE, 2003), pp. 983–985.
[11]S. Gong, H. Shen, and N. S. Barker, IEEE Trans. Microwave Theory Tech. **59**, 894 (2011).
[12]J. Lou, Z. Zhao, Y. Ruixia, M. Lu, and X. Hu, in *IEEE Antennas and Propagation Society International Symposium*, *20-25 June 2004* (IEEE, 2004), pp. 2867–2870.
[13]H. T. Kim, J. H. Park, J. Yim, Y. K. Kim, and Y. Kwon, IEEE Microwave Wireless Compon. Lett. **12**, 324 (2002).
[14]A. Vahdati, M. Varonen, M. Kärkkäinen, and K. A. I. Halonen, in *9th Conference on Ph.D. Research in Microelectronics and Electronics*, *Villach, Austria*, *24-27 June 2013* (IEEE, 2013), pp. 97–100.
[15]H. T. Kim, J. H. Park, Y. K. Kim, and Y. Kwon, in *IEEE MTT-S International Microwave Symposium Digest*, *Seattle, USA*, *2-7 June 2002* (IEEE, 2002), pp. 341–344.
[16]J. A. Rubiño-Martin, R. Rebolo, M. Tucci, R. Génova-Santos, S. R. Hildebrandt, R. Hoyland, J. M. Herreros, F. Gómez-Renasco, C. López, E. Martínez-González, P. Vielva, D. Herranz, F. J. Casas, E. Artal, B. Aja, L. de la Fuente, J. L. Cano, E. Villa, A. Mediavilla, J. P. Pascual, L. Piccirillo, B. Maffei, G. Pisano, R. A. Watson, R. Davis, R. Davies, R. Battye, R. Saunders, K. Grainge, P. Scott, M. Hobson, A. Lasenby, G. Murga, C. Gómez, A. Gómez, J. Arino, R. Sanquirce, J. Pan, A. Vizcarguenaga, and B. Etxeita, in *Highlights of Spanish Astrophysics V, Astrophysics and Space Science Proceedings, Part III* (Springer, Berlin, 2010), pp. 127–135.
[17]M. López-Caniego *et al.*, "Instrumentation and methods for astrophysics," in *Conference Proceedings Rencontres du Vietnam 2013: Cosmology in the Planck Era* (ICISE, 2014), p. 1.
[18]A. M. Peláez, J. I. Alonso, P. Almorox, and J. González, Microwave J. **52**, 32 (2009).
[19]R. J. Hoyland, in *Proceedings of 3rd ESA Workshop on Millimetre Wave Technology and Applications*, *Espoo, Finland*, *21-23 May 2003*, edited by J. Mallat, A. Räisänen, and J. Tuovinen (European Space Agency, Paris, 2003), pp. 305–310.
[20]E. Villa, Ph.D. thesis, Universidad de Cantabria, Santander, Spain, 2014.
[21]S. H. Choi, J. Y. Lee, K. B. Lee, and D. H. Shin, in *Asia-Pacific Microwave Conference*, *Bangkok, Thailand*, *11-14 December 2007* (IEEE, 2007), pp. 1–4.

Reuse of AIP Publishing content is subject to the terms at: https://publishing.aip.org/authors/rights-and-permissions. Download to IP: 193.144.201.248 On: Thu, 29 Sep 2016 13:36:19